ULTRASONIC IMAGING OF 3D DISPLACEMENT VECTORS USING A SIMULATED 2D ARRAY AND BEAMSTEERING

R. J. Housden, A. H. Gee,
G. M. Treece and R. W. Prager

CUED/F-INFENG/TR 669

June 2011

University of Cambridge
Department of Engineering
Trumpington Street
Cambridge CB2 1PZ
United Kingdom

Email: rjh80/ahg/gmt11/rwp @eng.cam.ac.uk

Ultrasonic imaging of 3D displacement vectors using a simulated 2D array and beamsteering

R. James Housden, Andrew H. Gee, Graham M. Treece and Richard W. Prager

University of Cambridge
Department of Engineering
Trumpington Street
Cambridge CB2 1PZ

Abstract

Most quasi-static ultrasound elastography methods image only the axial strain, derived from displacements measured in the direction of ultrasound propagation. Displacement estimation in other directions is significantly less accurate, but can be improved by steering the ultrasound beam through multiple angles and combining displacements measured along the different beam directions. In this paper, we investigate beamsteering as a way to estimate the full 3D displacement vector over a volume, using a simulated 2D array to steer both laterally and elevationally. With simulated and *in vitro* data, we show that more accurate lateral and elevational displacements and strains can be obtained using beamsteering.

1 Introduction

Ultrasonic elastography is a technique for visualising mechanical properties of tissues. The subject of this paper is quasi-static elastography [7], which involves estimating the relative displacement from one image to the next while continually varying the compression in the tissue. It is usually only the axial displacements that are measured with high precision, because the RF data contains high resolution phase information in this direction. Axial strain is then calculated from the gradient of the axial displacement estimates. Variations in axial strain indicate relative tissue stiffness under the assumption that soft regions of the tissue will deform more than stiff regions. Several potential clinical uses of axial strain imaging have been identified [1, 2, 11].

Lateral (and in the case of 3D imaging, elevational) displacements are usually of secondary interest, but can be tracked at lower precision to improve the accuracy of the axial displacements. However, the full 3D displacement vector is of interest for measuring other mechanical properties of tissue, e.g. Poisson's ratio for poroelastography [10], total shear strain for imaging tumour bonding [13] and for estimating the elastic modulus [9].

In 2D imaging, tracking axial and lateral displacements only, multiple angle beamsteering has been shown to improve the accuracy of displacements perpendicular to the beam [3, 8, 12]. This involves acquiring multiple images over a region, each with a different steering angle, so that the tissue is imaged from several different directions. For each angle, displacements are measured by comparing with a corresponding steered image at a different compression. The measured displacement is the component of the actual displacement along the beam direction. The components from each angle are then combined to estimate the axial and lateral components of the displacement field. This is illustrated in Figure 1(a). Throughout this paper, the terms axial and lateral refer to the fixed vertical and horizontal directions in which we are trying to estimate displacements. The actual directions of measurements taken along and across the steered beam are referred to as the beam direction and off-beam direction.

Although there has been significant research into 2D beamsteering, the same principle can be extended to estimate the full 3D displacement vector over a volume using a 2D array probe. This would involve acquiring multiple volumes of data at different steering angles, with some volumes steered laterally and some elevationally (Figure 1(b)). In this paper, we demonstrate 3D displacement estimation using multiple beamsteered volumes and compare the accuracy to displacements obtained using a single unsteered volume. We present results from a simulation of
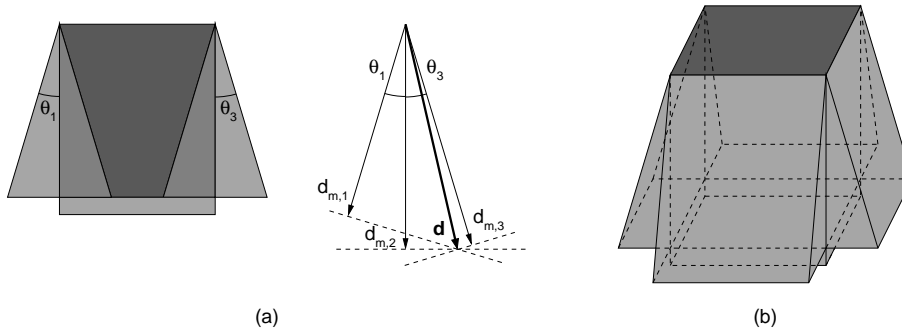
Figure 1: **Beamsteering principle**. (a) 2D beamsteering, with three laterally steered images at angles θ_1, θ_2 and θ_3. Here θ_1 and θ_3 are equal angles steering to the left and right and $\theta_2 = 0°$. The actual displacement vector of a point in the image, **d**, is measured as components $d_{m,1}$, $d_{m,2}$ and $d_{m,3}$ along the beam direction of each image. These measurements can be used to estimate both the axial and lateral components of **d**. (b) In 3D beamsteering, this principle is extended to five intersecting volumes, two steered laterally and two elevationally, which allow the 3D displacement vector to be estimated.

a 2D array probe and an *in vitro* experiment imitating a 2D array using a mechanically controlled 1D array probe.

2   Methods

2.1   Displacement estimation

Displacement estimation is by one of two methods. The unsteered method tracks displacements between a single pair of volumes with beams perpendicular to the transducer. The steered method uses multiple pairs of volumes, each at a different steering angle.

For each steered or unsteered volume pair, displacements along the beam direction are estimated using the Weighted Phase Separation method [6] and two-pass tracking strategy described in [14]. Each displacement estimate is accompanied by a precision estimate calculated from a weighted variance of phase differences between the pre- and post-compression RF data [6].

For the unsteered method the displacement measurements along the beam directly give the axial displacements. Lateral and elevational displacements are calculated during axial tracking, following the method in [14]. After each axial displacement estimate, the matching correlation is calculated at offsets of ± 1 vector off the beam in the lateral direction. Subvector lateral displacements are obtained by a quadratic fit to the correlation value at each lateral offset according to

$$d_l = \frac{\rho_{-1} - \rho_1}{2(\rho_{-1} - 2\rho_0 + \rho_1)}$$

where ρ_{-1}, ρ_0 and ρ_1 are correlations of the RF envelope data at -1, 0 and +1 vector offset respectively from the initial lateral alignment. d_l is the subvector location of the maximum correlation, giving the lateral displacement relative to the initial alignment. This is then repeated for the elevational displacements. Lateral and elevational tracking also improve the axial estimates, because the search range on the second tracking pass is initialised with the offsets found in the first pass.

In the steered method, the volume pair at each angle is initially processed separately using the phase-based tracking method in the beam direction. Off-beam displacement tracking is not used, because the non-orthogonal nature of the search directions in steered data means that searching in the off-beam direction also affects the estimate in the beam direction. The skewed grid of displacements and associated precision estimates are then linearly resampled to a regular Cartesian grid aligned with the unsteered volume.

Beam-direction displacements from the individual angles are then combined in a least squares solution for axial, lateral and elevational displacements, similar to the 3D solution in [12]. The measured displacements are estimates of the projections of the actual displacement onto the beam directions, so the set of equations to solve are $d_{m,i} = \mathbf{d}.\mathbf{u}_i$. $d_{m,i}$ is a measured displacement, $\mathbf{d} = [d_a, d_l, d_e]^T$ is a vector of the axial, lateral and elevational displacements that we are estimating, and $\mathbf{u}_i$ is a unit vector in the beam direction. In our implementation, each volume is steered in either the lateral or elevational direction, but not both at once. $\mathbf{u}_i$ is therefore $[\cos\theta_i, \sin\theta_i, 0]^T$ for volumes steered by θ_i laterally, $[\cos\phi_i, 0, \sin\phi_i]^T$ for volumes steered by ϕ_i elevationally and $[1, 0, 0]^T$ for an unsteered volume. The equations are solved according to the standard weighted linear least squares approach, with each measurement weighted by its associated precision estimate derived from the variance of phase differences.

To calculate strain from displacements in any one direction, we simply take the difference of the two estimates either side of each estimation location. This is followed by a gaussian smoothing filter in each of the three directions and weighted by the precision of each estimate. The gaussian has a standard deviation of one axial estimate spacing.

2.2   Experimental setup

The two displacement estimation methods were compared using simulated data and an *in vitro* scan performed with a mechanically controlled 1D array probe imitating a 2D array. For the simulation, we determined a displacement field between a compressed and an uncompressed state using finite element modelling (Abaqus 6.7, Simulia, Rhode Island, USA). The model was a 3D cylinder of radius 7 cm and height 3 cm. It comprised a single linear elastic material, of Young's modulus 10 kPa and Poisson's ratio 0.495. The probe face was modelled as a 35 mm × 35 mm square rigid compressor on the top surface of the model. In the compressed state, the compressor indented the top surface of the model by 0.3 mm (1% compression). Frictionless slip conditions were defined at the base of the model and in the contact region between the compressor and the top surface. All other surfaces were unconstrained.

RF ultrasound data were simulated using Field II [4, 5]. The probe was modelled as a 192 × 192 element fully-populated array with element spacing 0.245 mm. The transducer centre frequency was 8.5 MHz. Each A-line was sampled at 50 MHz over 1700 samples, giving a depth of 26.2 mm. Focusing for each line was achieved using a set of 32 × 32 active elements, with a transmit focus depth of 13 mm and dynamic receive focusing.

Multiple volumes of 128 × 128 A-lines and different steering angles were simulated. The angles used were ±12° and ±6° laterally and elevationally, as well as an unsteered volume, giving nine angles altogether. These volumes were simulated in both the compressed and uncompressed state, with the scatterer positions adjusted by the displacement in the finite element model for the compressed state. The simulated RF data then had Gaussian white noise added, reducing the SNR of the RF signal to 20 dB.

Displacements for each volume were measured using approximately equal aspect ratio 3D matching windows of 8 RF cycles along the beam and 5 vectors in the off-beam directions. Window spacing was 0.6 mm, so that each window overlapped the next by 40% of its length. Over the volume, this resulted in a grid of 44 windows axially and 64 windows laterally and elevationally.

For the *in vitro* scan, we used a ULA-OP (Università degli Studi di Firenze, Italy) scanner with a LA523 (Esaote, Genoa, Italy) linear array probe. The probe specification is similar to the parameters used for simulation, except that it is a 1D array probe with a fixed elevational focus. Also, each 2D image comprised 192 A-lines, focused using 64 active elements. Displacement estimation window sizes were the same as for the simulated data, with a grid of 42 windows axially and 96 windows laterally and elevationally.

Volumes were acquired by mounting the probe on a system of motorised linear slides (T-LSR300B, Zaber Technologies Inc., Vancouver, BC, Canada) and stepping the probe elevationally through 192 steps of 0.245 mm. At each elevational step, the probe was steered laterally through five angles: 0°, ±6° and ±12°. This created five volumes of 192 × 192 A-lines. The probe scanned through a 1.5 mm thick polyethelene compression plate of approximately 8 cm × 9 cm. The

compression plate was stationary during the probe's elevational sweep to represent the stationary face of a 2D array probe. To acquire the elevationally steered volumes, the scanning target and compression plate were rotated by 90° and the process repeated. Finally, a similar set of volumes were acquired with the compression plate and probe moved downwards by 0.5 mm to compress the phantom. The complete acquisition produced ten volumes at each compression, two of which were unsteered. For displacement estimation, only the first of these two was used, so that there were nine volumes available for the steered method and one volume for the unsteered method.

The rotation was achieved with the compressor and target standing on a turntable capable of rotating about a vertical axis with a precision of $0°1'$. The primary source of misalignment between volumes before and after rotation is the estimate of the location of the rotation axis. Before the main acquisition, this was calibrated by scanning a point target on the turntable at several different rotational positions. The resulting set of points defined a circle, with the centre giving the location of the rotation axis. We have found that this approach is capable of aligning the volumes to within about one lateral vector spacing. This is better than the resolution of the strain images (2 vector lateral and elevational window spacing) and is sufficient for our experiments measuring slowly varying displacement fields.

The scanning target was an agar cylinder with a height of approximately 3.5 cm and radius 5 cm. The applied displacement of 0.5 mm resulted in an overall compression of approximately 1.4% of the phantom height. Scattering was provided by a uniform distribution of aluminium oxide powder. Contact with the compression plate and the surface the phantom was resting on was made via a combination of water and ultrasound gel. This low-friction contact allowed the phantom to expand laterally and elevationally more easily as it was compressed.

3 Results and Discussion

Figure 2 shows axial, lateral and elevational displacement images on various slices through the volume for the simulated data, using both the steered and unsteered method and compared to the actual displacements from the finite element model. Equivalent images for the *in vitro* data are shown in Figure 3. Although there is no ground truth displacement data for the *in vitro* data, it is known that the overall compression was approximately 1.4% and it is reasonable to assume that the phantom material was incompressible. The expected lateral and elevational strains are therefore 0.7%, producing 0.34 mm expansion over the width of the image, or ±0.17 mm at the edges if there is zero displacement at the centre.

To measure quantitatively the accuracy of the displacement estimation, we compared the displacements from the simulated data to the known displacement field of the finite element model. Table 1 shows mean and standard deviation error values for each of the three directions using both the steered and unsteered methods. Values are calculated over all the displacement estimation windows in a 3D region of interest (ROI). The ROI includes only the estimates that are covered by all nine volumes, and excludes a margin of 1 mm at the edges of this overlap region. The region is outlined in one image of Figure 2.

For the *in vitro* data, we assume that the actual displacement field is smoothly varying within the phantom and high frequency variations in the measured displacement fields are due to measurement errors. We calculate the standard deviation of small grids ($3 \times 3 \times 3$) of displacement estimation windows, which we expect to have similar displacements. Low values therefore suggest smoother, more accurate displacement fields. We take multiple measurements of this kind throughout a region of interest and use their average as an indication of displacement quality. Results are shown in Table 2. The region of interest is defined in the same way as for the simulated data and is outlined in one image of Figure 3.

The simulated and *in vitro* data show similar results. As with 2D beamsteering, there is little advantage to using beamsteering for axial displacements, since the unsteered volume is sufficient to track displacements in this direction. For the lateral and elevational displacements, a smoother, less noisy displacement field is produced using multiple steering angles. This is confirmed by the numerical values in Tables 1 and 2. For the *in vitro* data, it appears that the phantom has

(a) Displacement fields

(b) Axial displacements, centre axial-lateral slice

(c) Lateral displacements, centre axial-lateral slice

(d) Elevational displacements, centre axial-elevational slice
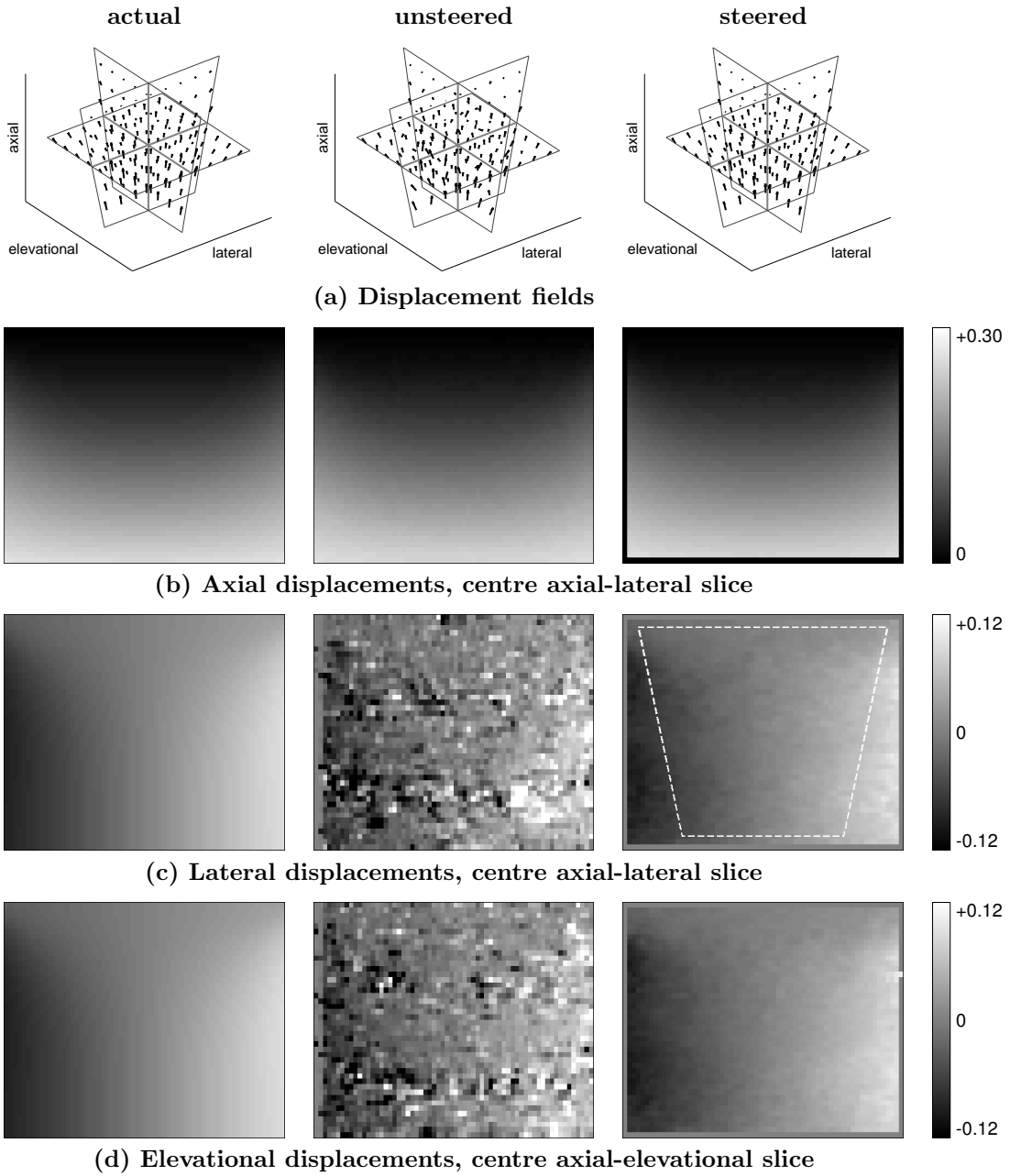
Figure 2: **Displacement images for simulated data**. (a) 3D vector fields of displacements on three orthogonal planes. (b–d) Axial, lateral and elevational displacement images for 2D slices through the volume. Values are in mm. The outline in the steered lateral image shows the extent of the 3D ROI used to calculate the values in Table 1.

unsteered **steered**

(a) Displacement fields

(b) Axial displacements, centre axial-lateral slice

(c) Lateral displacements, centre axial-lateral slice

(d) Elevational displacements, centre axial-elevational slice
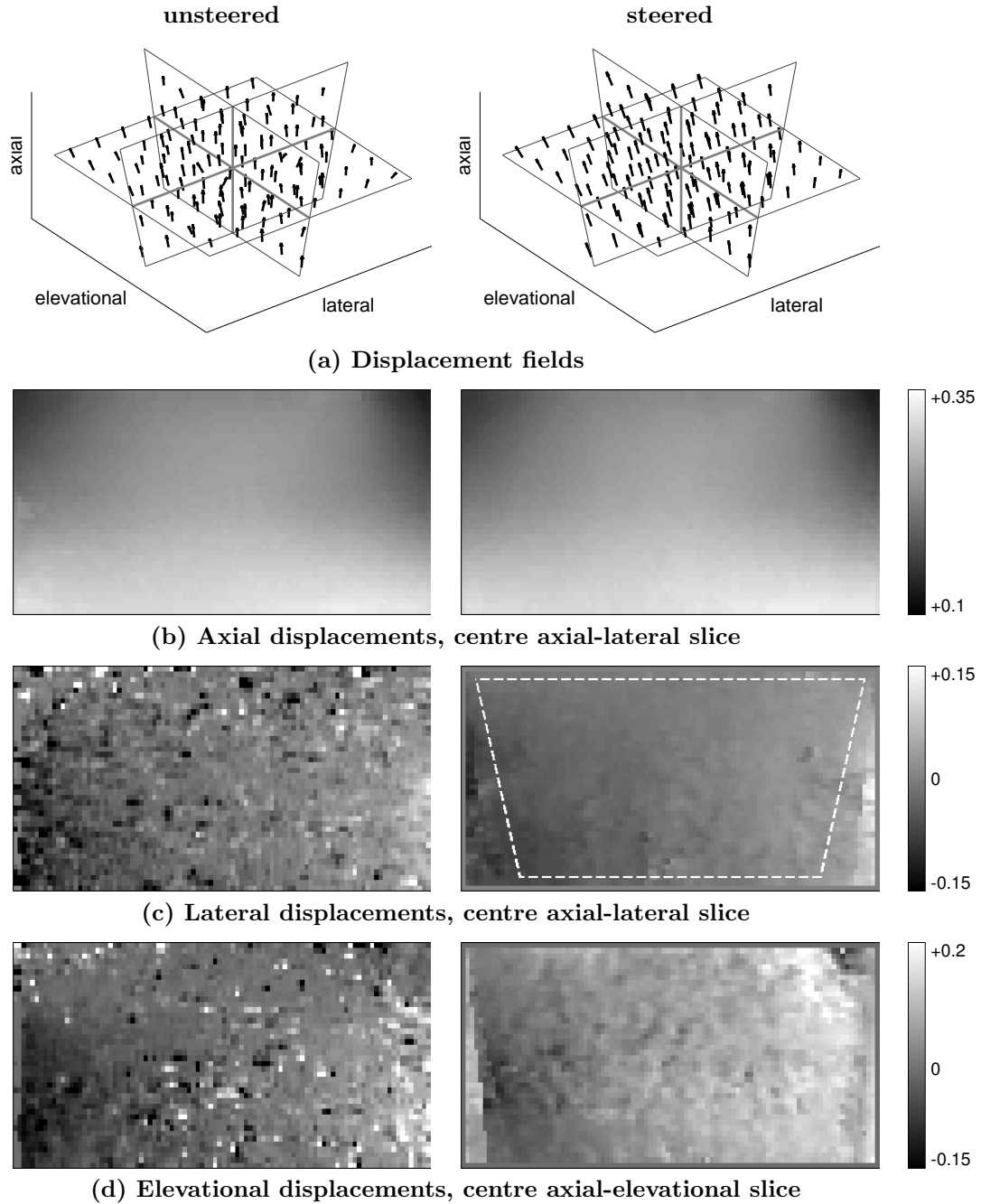
Figure 3: **Displacement images for *in vitro* data**. (a) 3D vector fields of displacements on three orthogonal planes. (b–d) Axial, lateral and elevational displacement images for 2D slices through the volume. Values are in mm. The outline in the steered lateral image shows the extent of the 3D ROI used to calculate the values in Table 2.

	unsteered	steered
axial	0.30 ± 1.27	0.92 ± 1.02
lateral	-0.12 ± 35.70	-0.67 ± 3.60
elevational	-0.52 ± 35.32	-0.52 ± 3.62

Table 1: **Displacement estimation error in simulated data**. Values are in μm, and show mean $\pm$ standard deviation. Errors are relative to ground truth displacements from the finite element model. The standard deviation is of most interest, since this is what affects the accuracy of strain calculated from the gradient of the displacements.

	unsteered	steered
axial	3.06	3.03
lateral	25.43	5.93
elevational	29.51	11.82

Table 2: **Displacement variation in *in vitro* data**. The values are averages of standard deviations of displacements, given in μm. The standard deviation is calculated on $3 \times 3 \times 3$ grids of displacement estimation windows and averaged over several of these grids. Since actual displacements are likely to be slowly varying and continuous, lower values suggest smoother and more accurate displacements.

expanded more elevationally than laterally and the elevational displacements are noisier as a result. This is most likely caused by imperfect slip conditions in the experimental setup.

The improved precision provided by beamsteering is particularly important for applications that require lateral and elevational strain, because even small imprecisions in the displacements become more significant when taking the gradient to measure strain. Figure 4 shows axial, lateral and elevational strain images for the *in vitro* data. Table 3 shows the average values of the elastographic signal to noise ratio (SNR_e) calculated over the same ROI as above. SNR_e is defined as mean divided by standard deviation for each $3 \times 3 \times 3$ grid of values in the ROI. Even with beamsteering, the lateral and elevational strain is clearly noisier than the axial strain. However, the beamsteered approach, with some post-processing from the gaussian filters, has produced reasonable lateral and elevational strain images. These may prove to be useful for volumetric imaging of other mechanical properties of tissue such as Poisson's ratio or total shear strain. For example, it has been noted that the accuracy of Poisson's ratio images is limited by the poor quality of lateral strain [10].

In this paper, we have demonstrated the principle of 3D beamsteering from a 2D array using simulated and *in vitro* data. A particular limitation of our *in vitro* setup is the inability to steer along more than one axis at once. An interesting future investigation would therefore be to experiment with different combinations of beams steered in any direction. Also, while our simulation represents a fully-populated 2D array with ideal transmit and receive focusing, the *in vitro* setup is limited by having used a 1D array with a fixed focus in the probe's elevational direction. A genuine 2D array with more typical focusing would be required to implement the beamsteering method in practice and verify the findings of our experiments. In addition, the method relies on each steering angle measuring displacements over the same compression. A practical implementation would therefore require a 2D array with a fast volume acquisition rate,

	unsteered	steered
axial	9.31	10.02
lateral	0.42	1.39
elevational	0.46	1.34

Table 3: **Mean SNR_e of strain**. The values are the averages of multiple SNR_e measures over $3 \times 3 \times 3$ grids of strain estimates within the ROI. Higher values indicate less noisy strain data.

unsteered **steered**

Axial strain, centre axial-lateral slice

Lateral strain, centre axial-lateral slice

Elevational strain, centre axial-lateral slice
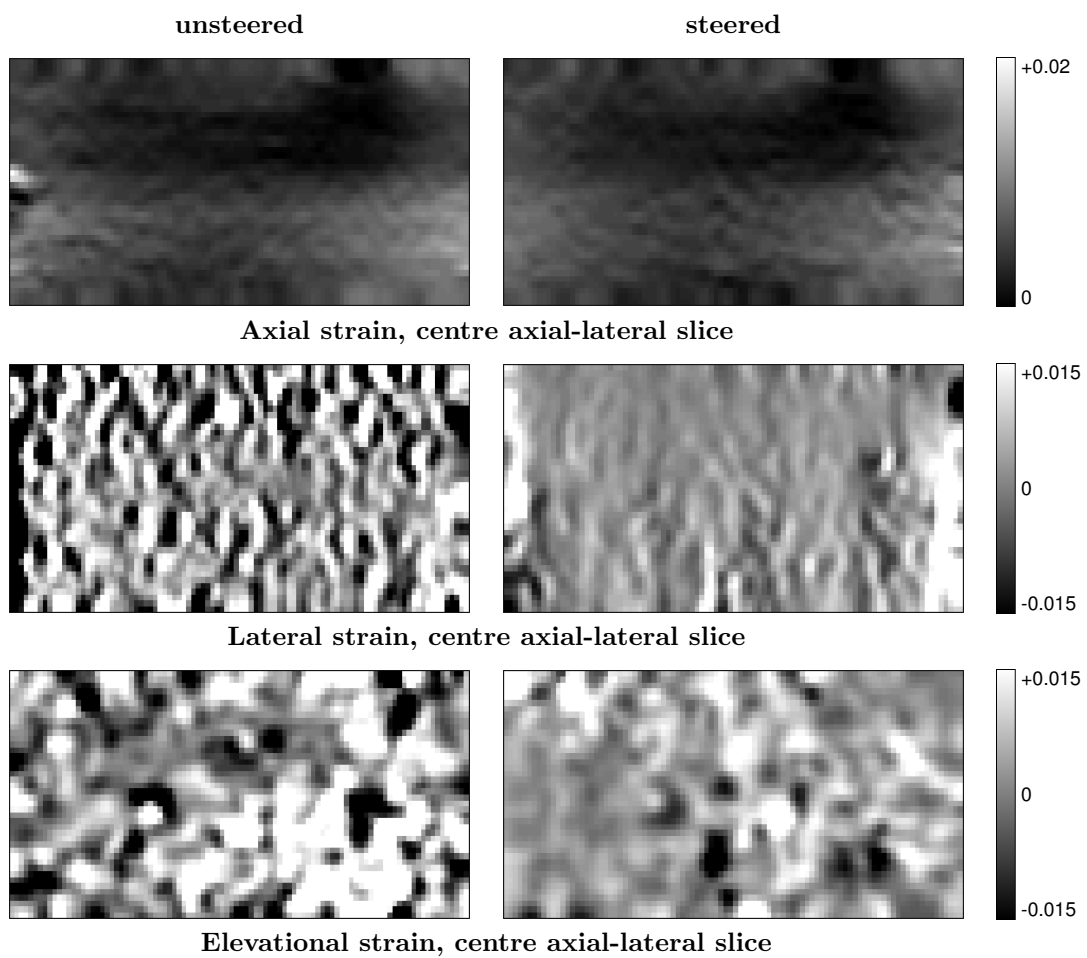
Figure 4: **Strain images for *in vitro* data**. The figure shows axial, lateral and elevational strain images on an axial-lateral slice through the volume.

so that the probe and tissue can be assumed to be stationary while several volumes are acquired at different angles. Under these conditions, it would be possible to acquire volumetric data suitable for estimating the full 3D displacement vector in more practical scenarios, including *in vivo* scanning.

4   Conclusions

We have presented a method for measuring full 3D displacement vector fields using multiple angle beamsteering from a 2D array probe. The superior displacement measurements along the beam direction give improved precision in the lateral and elevational directions. This translates to less noisy strain data in these directions. Although calculating other mechanical properties is beyond the scope of this paper, a more accurate measure of 3D displacement or strain is expected to improve such measures.

References

[1] E. S. Burnside, T. J. Hall, A. M. Sommer, G. K. Hesley, G. A. Sisney, W. E. Svensson, J. P. Fine, J. Jiang, and N. J. Hangiandreou. Differentiating benign from malignant solid breast masses with US strain imaging. *Radiology*, 245(2):401–410, November 2007.

[2] B. S. Garra, E. I. Cespedes, J. Ophir, S. R. Sprat, R. A. Zuurbier, C. M. Magnant, and M. F. Pennanen. Elastography of breast lesions: initial clinical results. *Radiology*, 202(1):79–86, January 1997.

[3] H. H. G. Hansen, R. G. P. Lopata, T. Idzenga, and C. L. de Korte. Full 2D displacement vector and strain tensor estimation for superficial tissue using beam-steered ultrasound imaging. *Physics in Medicine and Biology*, 55(11):3201–3218, June 2010.

[4] J. A. Jensen. Field: a program for simulating ultrasound systems. In *Proceedings of the 10th Nordic-Baltic conference on Biomedical Imaging*, pages 351–353, Tampere, Finland, June 1996.

[5] J. A. Jensen and N. B. Svendsen. Calculation of pressure fields from arbitrarily shaped, apodized, and excited ultrasound transducers. *IEEE Transactions on Ultrasonics, Ferroelectrics, and Frequency Control*, 39(2):262–267, March 1992.

[6] J. E. Lindop, G. M. Treece, A. H. Gee, and R. W. Prager. Phase-based ultrasonic deformation estimation. *IEEE transactions on Ultrasonics, Ferroelectrics, and Frequency Control*, 55(1):94–111, January 2008.

[7] J. Ophir, I. Céspedes, H. Ponnekanti, Y. Yazdi, and X. Li. Elastography: a quantitative method for imaging the elasticity of biological tissues. *Ultrasonic Imaging*, 13(2):111–134, April 1991.

[8] M. Rao, Q. Chen, T. Shi, T. Varghese, E. L. Madsen, J. A. Zagzebski, and T. A. Wilson. Normal and shear strain estimation using beam steering on linear-array transducers. *Ultrasound in Medicine and Biology*, 33(1):57–66, January 2007.

[9] M. S. Richards, P. E. Barbone, and A. A. Oberai. Quantitative three-dimensional elasticity imaging from quasi-static deformation: a phantom study. *Physics in Medicine and Biology*, 54(3):757–779, February 2009.

[10] R. Righetti, S. Srinivasan, A. Thitai Kumar, J. Ophir, and T. A. Krouskop. Assessing image quality in effective Poisson's ratio elastography and poroelastography: I. *Physics in Medicine and Biology*, 52(5):1303–1320, March 2007.

[11] R. Souchon, O. Rouvière, A. Gelet, V. Detti, S. Srinivasan, J. Ophir, and J-Y. Chapelon. Visualisation of HIFU lesions using elastography of the human prostate in vivo: preliminary results. *Ultrasound in Medicine and Biology*, 29(7):1007–1015, July 2003.

[12] U. Techavipoo, Q. Chen, T. Varghese, and J. A. Zagzebski. Estimation of displacement vectors and strain tensors in elastography using angular insonifications. *IEEE Transactions on Medical Imaging*, 23(12):1479–1489, December 2004.

[13] A. Thitai Kumar, J. Ophir, and T. A. Krouskop. Noise performance and signal-to-noise ratio of shear strain elastograms. *Ultrasonic Imaging*, 27(3):145–165, July 2005.

[14] G. M. Treece, J. E. Lindop, A. H. Gee, and R. W. Prager. Freehand ultrasound elastography with a 3-D probe. *Ultrasound in Medicine and Biology*, 34(3):463–474, March 2008.